Interpreting *in situ* x-ray diffraction data from high pressure deformation experiments using elastic–plastic self-consistent models: an example using quartz

2008 J. Phys.: Condens. Matter 20 285201

(http://iopscience.iop.org/0953-8984/20/28/285201)

IOP PUBLISHING JOURNAL OF PHYSICS: CONDENSED MATTER

J. Phys.: Condens. Matter **20** (2008) 285201 (10pp) doi:10.1088/0953-8984/20/28/285201

Interpreting *in situ* x-ray diffraction data from high pressure deformation experiments using elastic–plastic self-consistent models: an example using quartz

P C Burnley[1] **and D Zhang**

Department of Geosciences, Georgia State University, Atlanta, GA 30302-4105, USA

E-mail: Pamela.Burnley@unlv.edu

Received 9 January 2008, in final form 30 April 2008
Published 13 June 2008
Online at stacks.iop.org/JPhysCM/20/285201

Abstract

We present synchrotron x-ray diffraction observations from a deformation experiment on fine-grained polycrystalline quartz using the newly developed deformation DIA apparatus. During deformation experiments we were able to observe the elastic strain of the (100), (101) and (112) lattice reflections. The elastic strains are typically converted into stresses and interpreted in terms of the differential stress supported by the specimen. Consistently with results from others obtained using this technique to deform monomineralic polycrystals, our results show substantial variations in stress levels between grain populations. Rather than averaging the lattice reflection stresses or choosing a single reflection to determine the macroscopic stress supported by the specimen, we explore the use of elastic–plastic self-consistent (EPSC) models. We are able to match the measured differential elastic lattice strains with an EPSC model in which basal and prism $\langle a \rangle$ slips are activated. An interesting outcome of the EPSC model is the prediction that the macroscopic stress experienced by the sample should be greater than the stress calculated from any of the reflections that we observed. This observation serves as a caution against using reflection stresses as a proxy for the macroscopic stress in *in situ* deformation experiments.

(Some figures in this article are in colour only in the electronic version)

1. Introduction

The rheology of Earth materials governs many aspects of Earth's behaviour from mountain building to the mixing of geochemical reservoirs in the mantle and is therefore a very important field of investigation. Unfortunately, quantitative deformation studies at conditions relevant to the earth's interior have been plagued with technical challenges. At very low pressure (0.3 GPa), high precision deformation experiments are possible using a gas apparatus (Paterson 1990). The Griggs apparatus, a modified piston cylinder apparatus, achieves higher pressures by using solid confining media. However, friction between the solid confining media and the sample and deformation pistons compromises the precision of the stress measurements, which are made with an external load cell. Friction between the sample and cell parts has been ameliorated by the use of molten salt cells (Green and Borch 1989, Gleason and Tullis 1993), but the Griggs apparatus is still limited to confining pressures of <4 GPa. The extrusion of samples from between the anvils of a diamond anvil cell (DAC) has been used to study deformation at very high pressures (e.g. Meade and Jeanloz 1988, Merkel *et al* 2006).

[1] Author to whom any correspondence should be addressed. Present address: High Pressure Science and Engineering Center, University of Nevada, Las Vegas, Box 454002, 4505 Maryland Parkway, Las Vegas, NV 89154-4002, USA.

However, DAC samples are very small, and the stress and strain fields are complex which has limited the interpretive power of the results. Recent technological developments in high pressure apparatus for controlled deformation (including the deformation DIA (D-DIA) (Durham *et al* 2002, Wang *et al* 2003), the rotational Drickamer apparatus (RDA) (Yamazaki and Karato 2001) and a belt type deformation apparatus (Dobson *et al* 2005)) have opened an increasing range of pressures over which quantitative deformation experiments may be conducted. These apparatus rely on *in situ* diffraction (either synchrotron x-ray or neutron) to monitor the state of stress in the sample. In the case of the synchrotron experiments, the stress analysis technique utilizes differential strains of individual lattice planes to calculate the sample stress. This method is also used for analysing stress in DAC experiments (Singh *et al* 1998).

A major challenge is that the diffraction data from the new high pressure deformation experiments reveal a more complex picture of polycrystalline deformation than was anticipated (Li *et al* 2004). Stress levels calculated from different x-ray reflections have been shown to substantially disagree (Li *et al* 2004, Mei *et al* 2003, 2005, Weidner and Li 2006). This is because the diffraction data is generated by individual grains in the polycrystal and therefore reflects grain scale phenomena rather than macroscopic properties. It is therefore not immediately obvious to how derive the macroscopic stress supported by the sample from the stresses measured in the grains. Determining the method to properly interpret the diffraction data and to cast it in terms of macroscopic stresses is important because it is the aggregate properties that are useful for geodynamic calculations. Fortunately, significant progress towards this goal has already been made by metallurgists who use neutron diffraction to study the deformation of metals at room pressure. One of the methods that they have developed is elastic–plastic self-consistent (EPSC) modelling. In this paper, we present diffraction data from polycrystalline quartz deformed at 2 GPa and 800 °C. We compare the observed diffraction with predictions from an EPSC model of deforming polycrystalline quartz and discuss the advantage of such an approach.

2. Experimental technique

2.1. D-DIA apparatus

Experiments were carried out in the D-DIA apparatus (Durham *et al* 2002, Wang *et al* 2003), a modified version of the DIA apparatus (Osugi *et al* 1964, Shimomura *et al* 1985) that uses 6 hard anvils (primarily WC) to compress a cube-shaped sample assembly. The anvils are driven inwards by two wedged guide blocks that are forced together by a large hydraulic press. In the DIA apparatus the anvils advance at the same rate, but in the D-DIA small hydraulic rams incorporated in the guide blocks allow the top and bottom anvils to be advanced independently (Durham *et al* 2002, Wang *et al* 2003). Our deformation experiments were conducted using the D-DIA apparatus installed in the SAM85 press in the X17B2 hutch at National Synchrotron Light Source at Brookhaven National Laboratory.

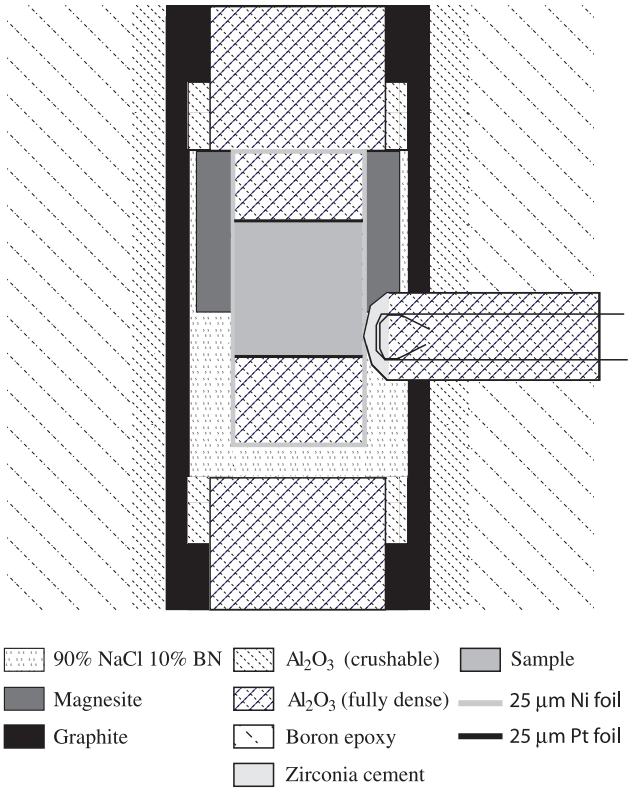

Figure 1. D-DIA sample assembly. The pressure medium consists of a 6 mm cube of boron epoxy. The interior consists of nested sleeves surrounding a cylindrical sample. The thermocouple is introduced through a hole drilled into the side of the assembly. The function of each material included in the assembly is discussed in the text.

The sample assembly (figure 1) consisted of a cubic volume of boron epoxy, a soft material that serves as the confining medium, with a cylindrical graphite furnace in the centre. A W3%Re–W25%Re thermocouple was introduced from the side to measure the sample temperature. The sample was surrounded by an additional sleeve of ductile confining medium inside the furnace and enclosed in a 25 μm thick Ni metal jacket. The confining medium sleeve consisted of two parts. The lower portion was composed of 90% NaCl 10% BN. NaCl is commonly used as a confining medium in Griggs apparatus sample assemblies because of its low strength. For diffraction measurements it has the additional advantage of being relatively compliant which makes it a precise pressure calibrant in the 2–3 GPa range. The Decker equation of state (Brown 1999) was used to determine pressure in the NaCl. The BN was used to suppress grain growth. The upper portion of the confining medium sleeve was composed of a split sleeve of magnesite that served as an x-ray window. Magnesite has diffraction peaks that are far enough away from those of quartz so as not to overlap or interfere. The strength of magnesite is expected to be comparable to that of calcite, which is soft compared to quartz. In addition, the sleeve was split to allow the salt to intrude between the halves in order to minimize any lateral constraints placed on the sample by the sleeve. Above and below the sample, alumina pistons were used to transmit the load from the top and bottom anvils to the sample. We used

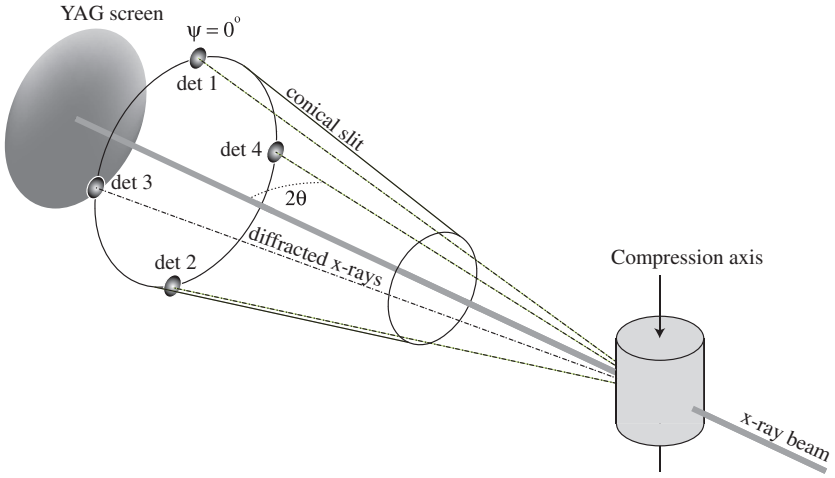

Figure 2. Diffraction geometry for D-DIA experiments. For clarity, the apparatus is not shown but the direction of the compression axis and the sample are shown along with the orientation of the incoming x-ray beam and the position of the four detectors and the YAG screen. The conical slit that excludes x-rays diffracting at angles other than 2θ is shown schematically.

a layer of Pt between the sample and the pistons as a strain marker. The sample material was Arkansas novaculite, a pure quartz aggregate with a grain size of 6–9 μm.

2.2. In situ x-ray measurements

White x-rays enter and leave the sample assembly along a direction perpendicular to the compression axis via the spaces between the side anvils. Transparent anvil tips (cubic BN) are used on the side anvils to allow the diffracted x-rays to be observed at a variety of angles. At X17B2 the diffracted x-rays are measured using four energy dispersive detectors (figure 2). Two of the detectors (det 1 and det 2) measure diffraction from crystallographic planes that are nearly perpendicular to the compression direction. The other detectors (det 3 and det 4) measure diffraction from crystallographic planes that are very close to a plane defined by the direction of the x-ray beam and the compression direction. The small angular differences are due to the diffraction angle which is ∼3.25°. The pairs of detectors measure redundant information which is valuable both for alignment and for data quality control. A conical slit (Durham *et al* 2002) that sits up-stream of the detectors, determines the two theta angle of the diffracted x-rays and eliminates most of the diffraction from the sample assembly. Because the x-ray source is white, there will be a wavelength that fulfils the Bragg condition for each set of lattice planes in the sample. Thus each detector measures a full powder pattern from the sample as well as from the parts of the sample assembly in the region from which diffraction is observed (this generally includes the confining medium inside the furnace but not the furnace itself). Lattice spacings are determined from the diffraction pattern via calibration spectra that are collected at the start of each experiment. There is very little drift in the detector electronics so that calibration spectra collected 24–48 h apart are essentially identical.

Strain in the sample was measured by comparing the length of the sample in radiographic images made from the transmitted x-ray beam (Vaughan *et al* 2000, Li *et al* 2003). Radiographic images are achieved by photographing the fluorescence of a YAG screen that is located at the centre of the conical slit. Thin Pt metal foils above and below the sample absorb the direct beam allowing the dimensions of the sample (which is x-ray transparent) to be imaged.

2.3. Experimental procedure

The experiment was compressed cold to 1.5 GPa and then heated to 950 °C for a one hour soak, which allowed stress in the sample accumulated during cold loading to relax. The sample was then cooled to 27 °C at pressure in order to accommodate an interruption in the availability of the synchrotron beam. The sample was then heated to 800 °C and the deformation rams were advanced at a rate that produced a sample strain rate of 10^{-5} s^{-1}. A radiograph was taken before the rams started to advance and then alternating spectra from the sample and radiographs were taken. Initially a series of five 60 s spectra were taken in between each radiograph to capture the rapid changes in the stress state during elastic loading. Later spectra were collected for 300 s. When the sample reached 7% strain the power was quenched and the experiment depressurized. Once the press was opened spectra were collected from the sample and the alumina diffraction standard.

2.4. Data analysis

Peaks from the spectra (figure 3) were individually fit using Plot85 which uses a pseudo-Voigt peak fitting routine. To calculate differential lattice strains d-spacings from the detectors 1 and 2 and detectors 3 and 4 were averaged. The difference between detector 1 and detector 2 as well as the difference between detectors 3 and 4 is used as a measure of uncertainty. Macroscopic sample strain was determined from the distance between the Pt foils for each radiograph. The creation time of the image file was used as a proxy for the time at which the radiograph was taken since files were

saved within 10–20 s. The midpoint time of the spectra collection period was chosen as the time point associated with each spectra. The macroscopic strain associated with each spectra was determined by linear interpolation between strain/time data points. The sample began the deformation experiment experiencing a hoop stress due to the greater thermal expansivity of the salt relative to the quartz and alumina pistons. Therefore, we choose the average time when the d-spacings in all four detectors were equal to be the time at which strain was considered to be zero.

Stresses and pressures were calculated using the elastic constants and lattice parameters found in table 1. Although pressure during the experiment was determined from the NaCl pressure calibrant, for the analysis of the quartz spectra, we used the sample spectra to determine pressure. This was calculated using a third order Birch–Murnaghan equation of state applied to the unit cell volume as measured in each pair of detectors. The 'hydrostatic' pressure (P) was then calculated from $P = (P_3 + 2P_1)/2$ where P_1 is the pressure from detectors 3 and 4. P_3 is the pressure from detectors 1 and 2.

3. Results and discussion

The d-spacings for the (100), (101) and (112) reflections measured at each of the four detectors as a function of time during the deformation portion of the experiment are shown in figure 4. The calculated 'hydrostatic' d-spacing, $d_P^{hkl} = (d_3^{hkl} + 2d_1^{hkl})/3$ where d_1^{hkl} is the average d-spacing for detectors 3 and 4 and d_3^{hkl} is the average for detectors 1 and 2, is also plotted. When the rams first began to advance the d-spacings for detectors 3 and 4 were smaller than those observed in detectors 1 and 2. As mentioned above, we believe this state of stress was caused by the greater thermal expansion of the salt relative to the quartz and alumina. The 'hydrostatic' d-spacings decreased during the experiment reflecting the increase in mean stress as σ_3 increases but also a rise in pressure in the cell as the top and bottom anvils advance. The pressure recorded by the NaCl confining medium during the deformation rose from an initial value of 1.8 to 2 GPa. The uncertainty in d-spacing due to peak fitting is a small fraction of height of the plot symbol. This was evaluated by repeated fitting of peaks and by comparing the same peak fit by different individuals. Detector misalignment would cause systematic differences between pairs of detectors for all peaks—which is not observed. We interpret the differences in d-spacings observed in the pairs of detectors as reflecting random error associated with the finite number of grains contributing to each reflection.

3.1. Stress measurement from diffraction data

Stress measurement from diffracted x-rays is based upon the differences in lattice spacing measured as a function of the azimuthal angle, ψ, between the diffraction vector and loading direction (figure 2).

As discussed above, in our case, the x-rays enter the sample perpendicular to the compressive axis and leave the sample by a small diffraction angle, 2θ-where $\theta = 3.25°$. For a randomly oriented, fine-grained polycrystal under hydrostatic conditions, the d-spacings observed by all the detectors will be the same. Non-hydrostatic stress in the sample will cause

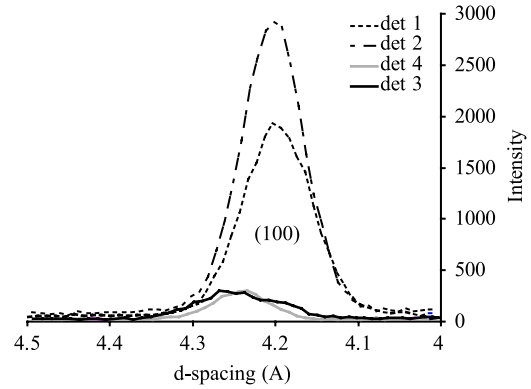

Figure 3. Example of (100) diffraction peak as measured in each detector at a macroscopic strain of 0.019. Spectra were collected for 60 s. The measured differential lattice strain is 0.0102.

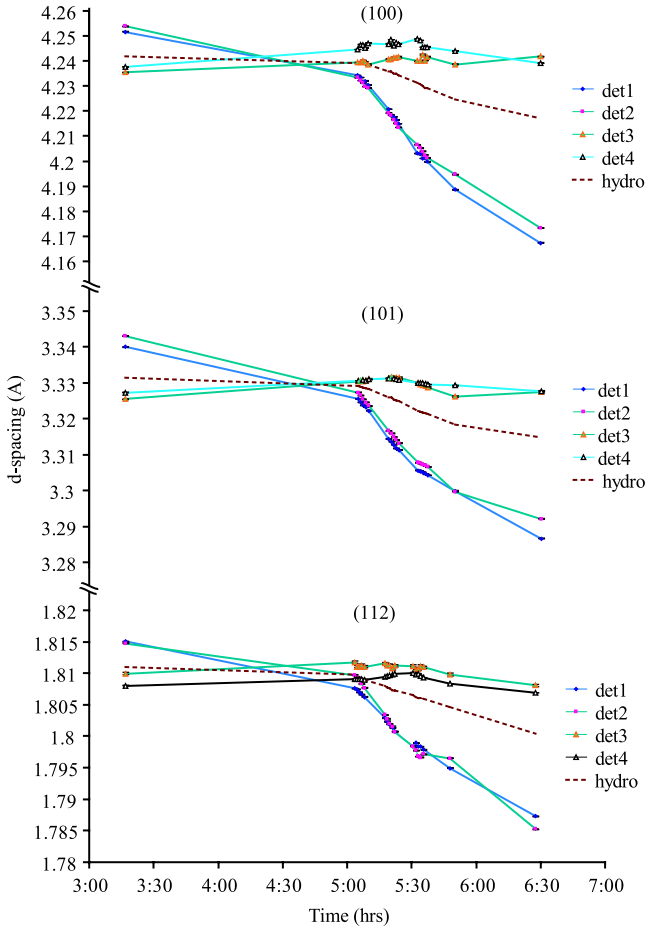

Figure 4. Lattice spacings for the (100), (101) and (112) reflections as a function of time during the deformation experiment. Detectors 1 and 2 measure diffraction from lattice planes that are nearly perpendicular to the compression direction. Detectors 3 and 4 measure diffraction from lattice planes that are parallel to the compression direction. The calculated 'hydrostatic' d-spacing is shown as a dashed line.

Table 1. Elastic constants and lattice constants used in calculations.

C_{11}	C_{33}	C_{44}	C_{12}	C_{13}	C_{14}
		(GPa)			
[a]87.7	[a]106.3	[a]59.0	[a]6.8	[a]12.3	[a]−18.7
dC_{11}/dT	dC_{33}/dT	dC_{44}/dT	dC_{12}/dT	dC_{13}/dT	dC_{14}/dT
		(GPa K^{-1})			
[a]−0.0076	[a]−0.0303	[a]−0.0153	[a]−0.0265	[a]−0.0124	[a]0.0
dC_{11}/dP	dC_{33}/dP	dC_{44}/dP	dC_{12}/dP	dC_{13}/dP	dC_{14}/dP
[b]3.28	[b]10.84	[b]2.66	[b]8.66	[b]5.97	[b]1.93
α_0	α_1	$K_0(T_0)$ (GPa)		K'	dK/dT (GPa K^{-1})
[c]9.3859×10^{-6}	[c]8.5404×10^{-8}	[d]37.12		[d]5.99	[a]−0.0153
a (Å)	c (Å)				
[e]4.91344	[e]5.40524				

[a] Quoted or derived from Ohno (1995).
[b] McSkimin *et al* (1965).
[c] Carpenter *et al* (1998).
[d] Angel *et al* (1997).
[e] LePage and Donnay (1976).

lattice spacings to vary as a function of their angular orientation in the sample. If the stress field experienced by each crystal is the same (a Reuss state) and if this field has cylindrical symmetry (as in the D-DIA) then difference in the d-spacing observed at $\psi = 0°$ and at 90° can be used as a measure of the differential stress supported by the polycrystal (Weidner *et al* 1992). This technique for stress measurement has become the standard method for calculating stresses from large-volume high pressure deformation experiments. Equations for calculating stresses from the differential strains of lattice planes using single crystal elastic constants have been derived for all crystal systems by Singh *et al* (1998).

For the subpopulation of grains contributing to a given reflection (hkl), the differential lattice strain is calculated from the average d-spacing for each set of detectors by:

$$\varepsilon^{hkl} = (d_1^{hkl} - d_3^{hkl})/d_P^{hkl}. \quad (1)$$

The subpopulation differential stress τ^{hkl}, defined as

$$\tau^{hkl} = \sigma_3^{hkl} - \sigma_1^{hkl}, \quad (2)$$

where σ_3^{hkl} and σ_1^{hkl} are the maximum and minimum compressive stresses, is calculated assuming a Reuss stress state, from ε^{hkl} by:

$$\tau^{hkl} = (2G_R^{hkl})\varepsilon^{hkl} \quad (3)$$

where $(2G_R^{hkl})^{-1}$ is the diffraction elastic constant. For point group 32 (for which $C_{52} = 0$) and our diffraction geometry, the diffraction elastic constant is calculated as

$$\begin{aligned}(2G_R^{hkl})^{-1} = {} & [(2S_{11} - S_{12} - S_{13}) \\ & + l_3^2(-5S_{11} + S_{12} + 5S_{13} - S_{33} + 3S_{44}) \\ & + l_3^4(3S_{11} - 6S_{13} + 3S_{33} - 3S_{44})]/2 \\ & + 3l_2l_3(3l_1^2 - l_2^2)S_{14} \end{aligned} \quad (4)$$

where $l_1 = \sqrt{3}ch/M$, $l_2 = c(h + 2k)/M$, $l_3 = \sqrt{3}al/M$, $M^2 = 4c^2(h^2 + hk + k^2) + 3a^2l^2$, h, k and l are the Miller indices of the lattice plane, and a and c are lattice parameters for the trigonal cell (Singh *et al* 1998). We obtained the elastic compliances S_{ij} through inverting the stiffness C_{ij} matrix which was calculated for the pressure and temperature of each spectra using the constants in table 1.

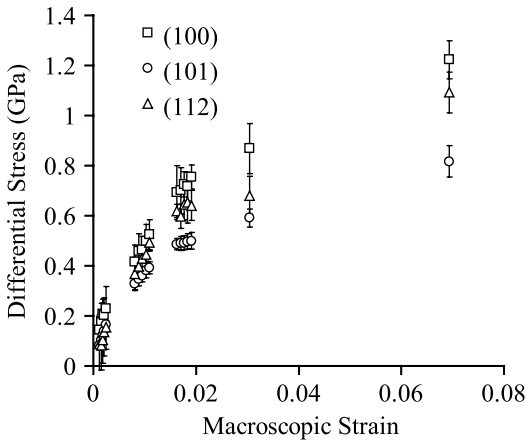

Figure 5. Differential stress calculated from the differential lattice strains for the (100), (101) and (112) reflections of quartz plotted versus the macroscopic strain. The macroscopic strain was determined by measuring the change in length of the sample recorded in radiographic images. The calculation assumes a Reuss state of stress in the polycrystal.

Figure 5 shows the calculated subpopulation differential stress (for an assumed Reuss state) for the quartz (100), (101) and (112) reflections in our experiment plotted versus macroscopic sample strain. The first feature one notices is that the stress calculated from each lattice reflection does not match the stress from the other lattice reflections and in fact, differ by a factor of 1.5. This wide variation in reflection stresses has also been observed in MgO (Li *et al* 2004, Weidner and Li 2006), fayalite olivine, (Chen *et al* 2006) and hcp-Co (Merkel *et al* 2006), and is attributed to the fact that plastic deformation places the state of stress outside of Reuss Voigt bounds (Li *et al* 2004, Weidner and Li 2006, Chen *et al* 2006).

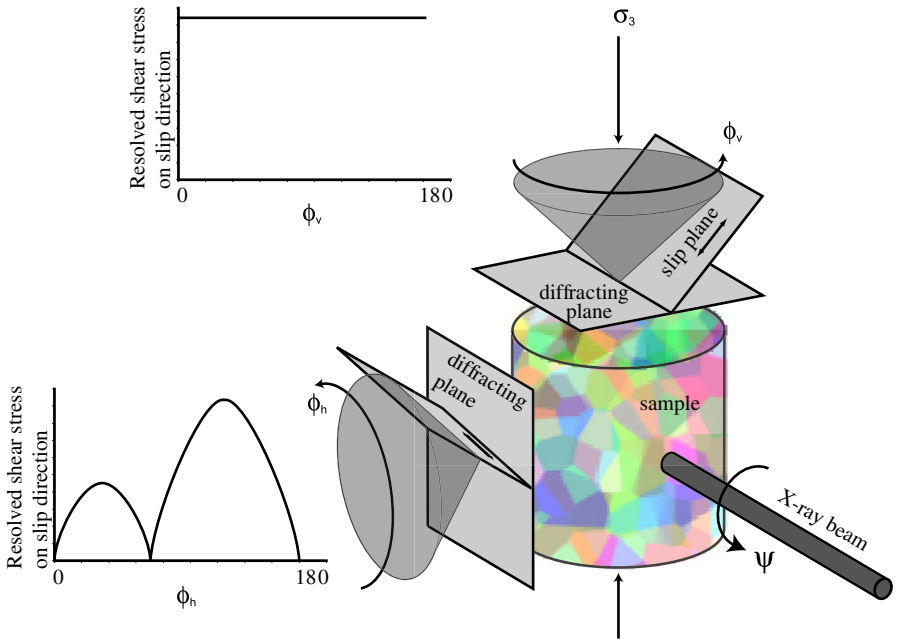

Figure 6. Diagram illustrating the relationship between the diffraction geometry for grains contributing to a given reflection and the orientation of a slip system within those grains. All grains contributing to the reflection in detectors 1 and 2 will experience the same resolved shear stress, where grains reflecting into detectors 3 and 4 will experience a variety of resolved shear stresses depending on their grain orientation.

Several questions arise from the results presented in figure 5 and those of other studies (e.g. Weidner and Li 2006, Chen *et al* 2006, Li *et al* 2004). First, what does it mean physically to be outside of the Voigt Reuss bounds? And second on a more practical note, how does one derive the true macroscopic load experienced by the sample from the variety of reflection stresses? In answer to the first question, it is important to recall that deformation, at the temperature at which this and many other D-DIA studies have been conducted, is controlled by dislocation glide. In a randomly oriented polycrystal some grains will be more favourably oriented for slip than others and the differential stress within those crystals will be lower than that in those crystals that are in a relatively hard orientation. In addition, crystals that have flowed will shift additional loads on to crystals in stronger orientations. Therefore, the assumption of a Reuss stress state is violated. Furthermore, the method by which stress is calculated assumes that the stresses in various grain populations that contribute to any given reflection observed in the pairs of detectors, are related in some simple way when in fact they are not. For grains diffracting into detectors 1 and 2 (ignoring the diffraction angle which is small), all grains contributing to a given reflection will experience the same resolved shear stress on their slip systems (figure 6). However, for any given reflection the resolved shear stress on the slip systems in contributing grains will be a function of the azimuthal angle ψ (between the diffraction vector and the loading direction). Furthermore, if the slip plane is not parallel to the diffracting plane, the resolved shear stress will also vary as a function of ϕ (the angle between the slip direction and the loading direction measured about the pole to the diffracting plane) (figure 6). Thus detectors 3 and 4 at $\psi = 90°$ may be measuring a population of grains in a variety of stress states. So for example, if the grains contributing to the reflection at $\psi = 0°$ are in a strong orientation and the majority of grains contributing to the reflection at $\psi = 90°$ are in a weak orientation, the differential stress calculated by comparing the d-spacings of these two populations would under estimate the macroscopic stress. One could easily imagine a scenario where the stress was over estimated instead. The complexity of analysing diffraction in the transverse direction has also been recognized by those using neutron diffraction to study deformation in metals (Daymond 2006, Oliver *et al* 2004).

From the discussion above, it is clear that the method we use for calculating stress from lattice strains needs to take plastic deformation into account. One such method is elastic–plastic self-consistent (EPSC) modelling. EPSC modelling also provides a means for calculating the macroscopic load experienced by the sample.

3.2. EPSC modelling

Self-consistent models provide an alternative method for calculating aggregate properties from single crystal elastic and plastic properties. First introduced by Kroner (1961), self-consistent models, are based on Eshelby's theory of inclusions (Eshelby 1957), which shows that an elliptical inclusion in a homogeneous matrix will experience uniform stress and strain. Elastic–plastic self-consistent models consider the elastic and plastic behaviour of a polycrystal by examining the behaviour of large numbers of individual grains. Each grain is treated as an elliptical inclusion within an infinite homogeneous matrix,

which in turn, has the average properties of all of the grains in the polycrystal. Each grain is described by its orientation, its single crystal elastic tensor and possible slip systems, each with its own critical resolved shear stress (CRSS). An increment of strain is applied to the homogeneous matrix that transmits stress to the grain. The grain responds elastically or plastically depending on its orientation and the CRSS of its slip systems, while also fulfilling compatibility criteria. The behaviour of the homogeneous matrix is the sum of the behaviours of the remainder of the grains and must be recalculated after each grain is deformed. Thus the model iterates until it converges for each deformation step. Work hardening may also be included in the model. Model output includes stresses and strains for each grain as well as average stress and elastic strains for populations of grains that contribute to various diffraction peaks. The macroscopic stress and strain for the aggregate are also calculated. Therefore, model results can be directly compared with diffraction results.

EPSC models were first employed for describing *in situ* diffraction observations (in this case, from neutrons) of deforming austenitic steel and copper by Clausen (1997). Clausen found that the behaviour of individual diffraction lines from the deforming steel (Clausen *et al* 1999) and copper were better described by an EPSC model rather than by an implementation of the Taylor or Sachs models. In particular, Clausen observed that lattice strains for individual reflections were no longer linear functions of the macroscopic strain once plastic deformation began. In addition, the deviation of the lattice strain from the macroscopic stain was different for each lattice reflection. The EPSC model was able to match this aspect of the behaviour and predict which reflections would experience more and less strain. EPSC models do not take into account grain to grain interactions, do not allow for rate dependence of plastic flow (for further discussion see Gloaguen *et al* 2006) and have not been successful in making quantitative predictions of the behaviour of individual diffraction lines (Daymond and Priesmeyer 2002, Daymond 2004). They do however, succeed in making qualitative predictions (±30%) of diffraction behaviour (Daymond 2004), and are reasonably successful in describing the evolution of LPO in deforming metals (Clausen 1997, Wang *et al* 2002). Furthermore, they have provided a powerful framework for the analysis of polycrystalline deformation (Daymond and Priesmeyer 2002). Self-consistent models are now commonly used to interpret neutron diffraction data from deforming metals (e.g. Agnew *et al* 2006, Daymond and Bonner 2003, Holden *et al* 2002, Cho *et al* 2002, Daymond *et al* 2000) including the partitioning of stress and strain between grains in two phase mixtures (Korsunsky *et al* 2002, Oliver *et al* 2004) and between matrix and included phases (Dye *et al* 2001). An EPSC model was used to fit differential elastic strains measured for deforming MgO at high pressure in a D-DIA (Li *et al* 2004, Chen *et al* 2006). In this study the ratio of CRSS for the slip systems was used to match the difference in differential lattice strains between the (111) and (200) reflections.

We used an EPSC code provided to us by C N Tome (Turner and Tome 1994) in order to interpret the diffraction results from our sample and estimate the macroscopic stress supported by the sample. Coding for trigonal symmetry was not implemented in this version of the code so hexagonal symmetry was used for the model. We tested a variety of models using the basal, prismatic ⟨*a*⟩ and rhomb ⟨*a*⟩ slip systems that are known to commonly operate in quartz. We modelled each slip system operating alone, in combinations of two and all three together. For each model we adjusted the CRSS and hardening slope for each slip system to obtain the best fit to the data. For basal and prismatic ⟨*a*⟩ slip operating alone we were not able to reproduce the observed yielding behaviour. The best fits for the other models are presented in figure 7. The CRSS and hardening slope used in each model are given in table 2. For models in which prismatic ⟨*a*⟩ slip is not operating (models 1 and 2) the (100) differential lattice strain overshoots the data by 3% strain. For models in which basal slip does not operate (models 1 and 3), the (112) differential lattice strain overshoots the data by 3% strain. The model that does the best job of matching the (100) differential lattice strain and also keeps the (101) and (112) differential lattice strains close together uses basal and prismatic ⟨*a*⟩ slip (model 4). Very similar results can be produced using all three slip systems (model 5). The basal slip system is known to be active at low temperatures with prismatic ⟨*a*⟩ slip and rhomb slip becoming active at somewhat higher temperatures (Kocks *et al* 1998, Tullis 2002). Hirth and Tullis (1994) observed microstructural evidence for basal and prismatic ⟨*a*⟩ slip operating in quartz at a similar temperature, pressure and strain rate. Figure 7(F) shows the macroscopic load associated with the 5 models shown in figure 7(A)–(E). The difference in the model macroscopic loads between the strongest and the weakest model is only 0.2 GPa (12%) at 7% strain and the difference between the model macroscopic loads for the two models that most closely reproduce the data only differ by 0.08 GPa (5%) at 7% strain.

Table 2. Parameters used in EPSC models shown in figure 7.

	Rhomb ⟨*a*⟩		Prismatic ⟨*a*⟩		Basal	
	CRSS (GPa)	Hardening slope	CRSS (GPa)	Hardening slope	CRSS (GPa)	Hardening slope
Model 1	0.12	1.6	Not activated		Not activated	
Model 2	0.13	1.6	Not activated		0.25	1.5
Model 3	0.13	1.6	0.22	0	Not activated	
Model 4	Not activated		0.15	0	0.16	1.8
Model 5	0.13	1.6	0.18	0	0.27	1.5

In order to illustrate the relationship between the macroscopic load and the reflection stresses we used model 4 to calculate reflection stresses for 10 quartz reflections with *d*-spacings greater than 1.65 Å; the region of the spectra that we can work with most readily. Note that these reflection stresses are not quite comparable to the reflection stresses plotted in figure 5 because those stresses were calculated assuming a Reuss state of stress. The reflection stresses along with the macroscopic stress are plotted in figure 8. Although individual reflection stresses are both larger and smaller than the macroscopic stress, the majority of reflections have lower stresses, including all three that we measured in our experiment. Four (including the (101) which is the most

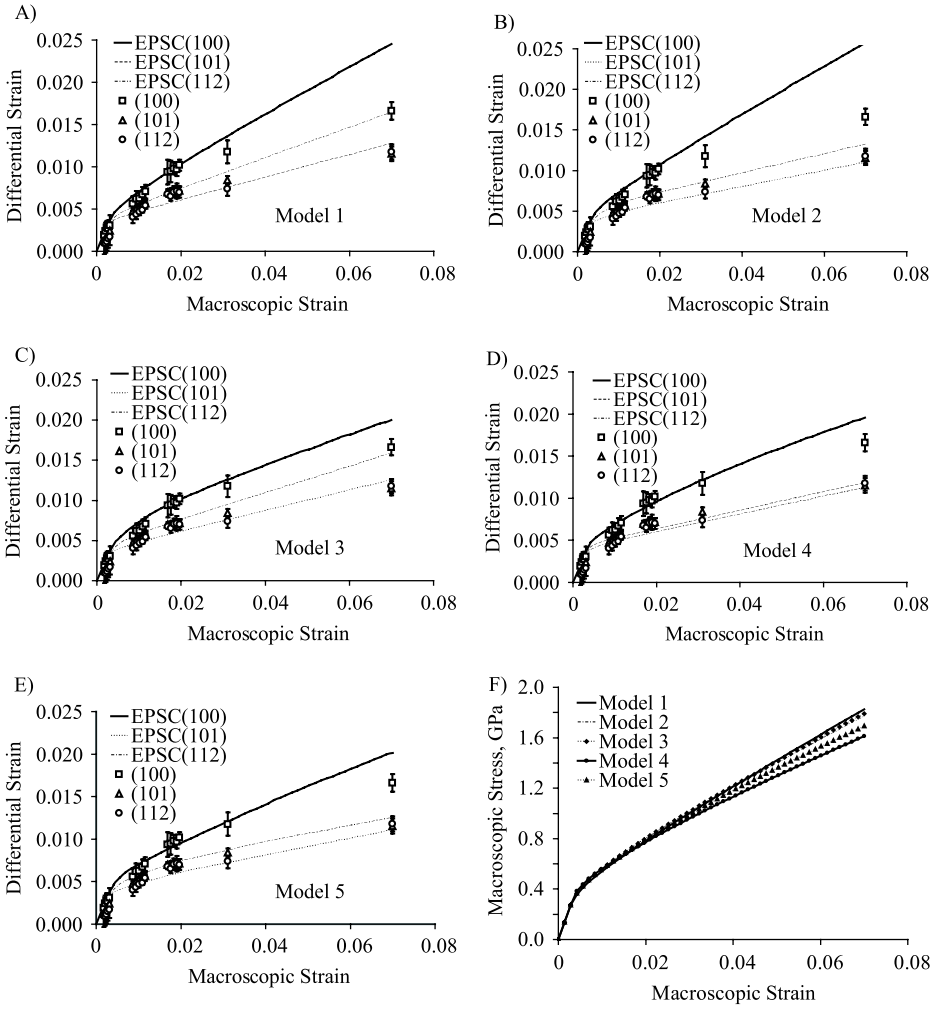

Figure 7. (A)–(E) Comparison of EPSC model results with observed differential lattice strains for the (100), (101) and (112) reflections of quartz. The parameters used in each model are listed in table 2. (F) shows the macroscopic stress supported by the sample for each of the models.

intense reflection in the quartz spectra) of the reflections are ∼0.5 GPa lower than the macroscopic stress. It is important to keep in mind that the macroscopic stress is governed by the cooperative behaviour of all the grains in the polycrystal but diffraction can only sample a small subset of the grains. The stress state in these grains my not be representative of the full population. Thus there is a serious hazard in taking the stress calculated from one or a small set of reflection (based on ease of measurement) as a proxy for the macroscopic load supported by the sample.

4. Conclusion

New *in situ* high pressure deformation techniques offer us an unprecedented way to examine the behaviour of polycrystalline materials at the grain scale during deformation. However, the derivation of macroscopic load on the specimen from reflection stresses is complicated by several factors. First, various subpopulations of diffracting crystals experience different levels of stress during deformation, which violates the Reuss assumption typically made in calculating reflection stresses from differential lattice strains. Secondly, reflection stresses

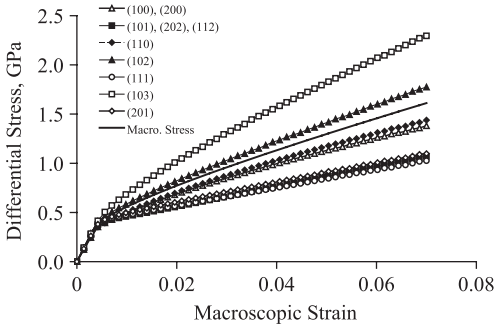

Figure 8. Differential stress calculated using EPSC model 4 (see table 2 for parameters used) for 10 quartz reflections. The calculated macroscopic stress supported by the sample is shown as a solid line. Note that most of the reflection stresses fall well below the macroscopic stress.

may give a poor approximation of the macroscopic stress if the full range of lattice reflection stresses is not measured. We believe that in order to properly interpret lattice strain data in terms of stress a model that takes the anisotropy of

plastic deformation into account is required. EPSC models, which have been extensively developed by metallurgists offer a good place to start at this task and offer a useful framework for testing hypothesis regarding deformation of polycrystalline materials at high pressure.

Acknowledgments

This work was supported by National Science Foundation grant EAR 01-36107 and partially supported by COMPRES, the Consortium for Materials Properties Research in Earth Sciences under NSF Cooperative Agreement EAR 01-35554 and EAR 06-49658. Use of the National Synchrotron Light Source, Brookhaven National Laboratory, was supported by the US Department of Energy, Office of Science, Office of Basic Energy Sciences, under Contract No. DE-AC02-98CH10886. The authors would like to thank undergraduate researchers Beth Lavoie, Mandi Reinshagen and Chris Collins for assistance with data collection and analysis as well as Liping Wang for assistance on the beam line. The authors would also like to acknowledge Don Weidner, Michael Vaughan, Carlos Tome and Jan Tullis for useful discussions and two anonymous reviewers for constructive critique.

References

Agnew S R, Brown D W and Tome C N 2006 Validating a polycrystal model for the elastoplastic response of magnesium alloy AZ31 using in situ neutron diffraction *Acta Mater.* **54** 4841–52

Angel R J, Allan D R, Miletich R and Finger L W 1997 The use of quartz as an internal pressure standard in high-pressure crystallography *J. Appl. Crystallogr.* **30** 461–6

Brown J M 1999 The NaCl pressure standard *J. Appl. Phys.* **86** 5801

Carpenter M A, Salje E K H, Graeme-Barber A, Wruck B, Dove M T and Knight K S 1998 Calibration of excess thermodynamic properties and elastic constant variations associated with the $\alpha \leftrightarrow \beta$ phase transition in quartz *Am. Mineral.* **83** 2–22

Chen J, Li L, Yu T, Long H, Weidner D J, Wang L and Vaughan M 2006 Do Reuss and Voigt bounds really bound in high-pressure rheology experiments? *J. Phys.: Condens. Matter* **18** S1049–59

Cho J R, Dye D, Conlon K T, Daymond M R and Reed R C 2002 Intergranular strain accumulation in a near-alpha titanium alloy during plastic deformation *Acta Mater.* **50** 4847–64

Clausen B 1997 Characterisation of polycrystal deformation by numerical modelling and neutron diffraction measurements *PhD Thesis* Riso National Laboratory Roskilde Denmark

Clausen B, Lorentzen T, Bourke M A M and Daymond M R 1999 Lattice strain evolution during uniaxial tensile loading of stainless steel *Mater. Sci. Eng.* A **259** 17–24

Daymond M R 2004 The determination of a continuum mechanics equivalent elastic strain from the analysis of multiple diffraction peaks *J. Appl. Phys.* **96** 4263–72

Daymond M R 2006 Internal stresses in deformed crystalline aggregates *Rev. Miner. Geochem.* **63** 427–58

Daymond M R and Bonner N W 2003 Lattice strain evolution in IMI 834 under applied stress *Mater. Sci. Eng.* **340** 272–80

Daymond M R and Priesmeyer H G 2002 Elastoplastic deformation of ferritic steel and cementite studied by neutron diffraction and self-consistent modelling *Acta Mater.* **50** 1613–26

Daymond M R, Tome C N and Bourke M A M 2000 Measured and predicted intergranular strains in textured austenitic steel *Acta Mater.* **48** 553–64

Dobson D P, Mecklenburgh J, Alfe D, Wood I G and Daymond M R 2005 A new belt-type apparatus for neutron-based rheological measurements at gigapascal pressures *High Pressure Res.* **25** 107–18

Durham W B, Weidner D J, Karato S and Wang Y 2002 New developments in deformation experiments at high pressure *Reviews in Mineralogy and Geochemistry: Plastic Deformation of Minerals and Rocks* vol 51 (Washington, DC: Mineralogical Society of America) pp 21–49

Dye D, Stone H J and Reed R C 2001 A two phase elastic-plastic self-consistent model for the accumulation of microstrains in waspaloy *Acta Mater.* **49** 1271–83

Eshelby J D 1957 The determination of the elastic field of an ellipsoidal inclusion and related problems *Proc. R. Soc.* A **241** 376–96

Gleason G C and Tullis J 1993 Improving flow laws and piezometers for quartz and feldspar aggregates *Geophys. Res. Lett.* **20** 2111–4

Gloaguen D, Berchi T, Girard E and Guillen R 2006 Prediction of intergranular strains using a modified self-consistent elastoplastic approach *Phys. Status Solidi* **203** R12–4

Green H W II and Borch R S 1989 A new molten salt cell for precision stress measurement at high pressure *Eur. J. Mineral.* **1** 213–9

Hirth G and Tullis J 1994 The brittle-plastic transition in experimentally deformed quartz aggregates *J. Geophys. Res.* **99** 11731–47

Holden T M, Holt R A and Pang J W L 2002 Intergranular stresses in ZIRCALOY-2 *Metall. Mater. Trans.* **33** 749–55

Kocks U F, Tomé C and Wenk H R 1998 Texture and Anisotropy *Preferred Orientations in Polycrystals and their Effect on Materials Properties* (Cambridge: Cambridge University Press) p 676

Korsunsky A M, Daymond M R and James K E 2002 The correlation between plastic strain and anisotropy strain in aluminium alloy polycrystals *Mater. Sci. Eng.* A **334** 41–8

Kroner E 1961 Zur plastischen verformung des vielkristalls (on the plastic deformation of polycrstals) *Acta Metall.* **9** 155–61

LePage Y and Donnay G 1976 Refinement of crystal structure of low-quartz *Acta Crystallogr.* B **32** 2456–69

Li L, Raterron P, Weidner D J and Chen J H 2003 Olivine flow mechanisms at 8 GPa *Phys. Earth Planet. Int.* **138** 113–29

Li L, Weidner D J, Chen J H, Vaughan M T, Davis M and Durham W B 2004 X-ray strain analysis at high pressure: effect of plastic deformation in MgO *J. Appl. Phys.* **95** 8357–65

McSkimin H J, Andreatch P and Thurston R N 1965 Elastic moduli of quartz versus hydrostatic pressure at 25° and −195.8 *J. Appl. Phys.* **36** 1624–32

Meade C and Jeanloz R 1988 Yield strength of MgO to 40 GPa *J. Geophys. Res.* **93** 3261–9

Mei S, Durham W B and Kohlstedt D 2005 Experimental investigation of the creep behavior of olivine at high pressure up to 12 GPa *EOS Trans. Am. Geophys. Union* **86** (52) V42A-0327

Mei S, Durham W B and Wang Y 2003 Deformation of olivine at high pressures using the deformation-DIA *EOS Trans. Am. Geophys. Union* **84** (46) MR13B-08

Merkel S, Miyajima N, Antonangeli D, Fiquet G and Yagi T 2006 Lattice preferred orientation and stress in polycrystalline hcp-Co plastically deformed under high pressure *J. Appl. Phys.* **100** 023510

Ohno I 1995 Temperature variation of elastic properties of α-quartz up to the $\alpha-\beta$ transition *J. Phys. Earth* **43** 157–69

Oliver E C, Daymond M R and Withers P J 2004 Interphase and intergranular stress generation in carbon steels *Acta Mater.* **52** 1937–51

Osugi J, Shimizu K, Inoue T and Yasunami K 1964 A compact cubic anvil high pressure apparatus *Rev. Phys. Chem. Japan* **34** 1–6

Paterson M S 1990 Rock deformation experimentation *The Brittle-Ductile Transition in Rocks* (*Geophysical Monographs* vol 56) ed A G Duba (Washington, DC: AGU) pp 187–94

Shimomura O, Yamaoka S, Yagi Y, Wakatsuki M, Tsuji K, Kawamura H, Hamaya N, Fukuoga O, Aoki K and Akimoto S 1985 Multi-anvil type x-ray system for synchrotron radiation *Solid State Physics Under Pressure* ed S Minomura (Tokyo: Terra Scientific Publishing) pp 351–6

Singh A K, Balasingh C, Mao H, Hemley R J and Shu J 1998 Analysis of lattice strains measured under nonhydrostatic pressure *J. Appl. Phys.* **83** 7567–75

Tullis J 2002 Deformation of granitic rocks: experimental studies and natural examples *Reviews in Mineralogy and Geochemistry: Plastic Deformation of Minerals and Rocks* vol 51 (Washington, DC: Mineralogical Society of America) pp 51–95

Turner P A and Tome C N 1994 A study of residual stresses in zircaloy-2 with rod texture *Acta Metal. Mater.* **42** 4143–53

Vaughan M, Chen J, Li L, Weidner D J and Li B 2000 Use of x-ray imaging techniques at high pressure and high temperature for strain measurements *Science and Technology of High Pressure Proc. AIRAPT-17 MH Manghnani* ed W J Nellis and M F Nicol, pp 1097–8

Wang Y, Durham W B, Getting I C and Weidner D J 2003 The deformation-DIA: A new apparatus for high temperature triaxial deformation to pressures up to 15 GPa *Rev. Sci. Instrum.* **74** 3002–11

Wang Y D, Peng R L, Wang X-L and McGreevy R L 2002 Grain-orientation-dependent residual stress and the effect of annealing in cold-rolled stainless steel *Acta Mater.* **50** 1717–34

Weidner D J and Li L 2006 Measurement of stress using synchrotron x-rays *J. Phys.: Condens. Matter* **18** S1061–7

Weidner D J, Vaughan M T, Ko J, Wang Y, Liu X, Yeganeh-Haeri A, Pacalo R E and Zhao Y 1992 Characterization stress pressure and temperature in SAM85 A DIA type high pressure apparatus *High-Pressure Research: Application to Earth and Planetary Sciences* (*Geophysical Monographs* vol 67) pp 13–7

Yamazaki D and Karato S 2001 High pressure rotational deformation apparatus to 15 GPa *Rev. Sci. Instrum.* **72** 4207–11